ORIGINAL ARTICLE

Stable sodium metal anode enhanced by advanced electrolytes with SbF₃ additive

Wei Fang, Rui Jiang, Hao Zheng, Yi Zheng, Yi Sun, Xin Liang, Hong-Fa Xiang* , **Yue-Zhan Feng, Yan Yu***

Abstract The practical application of sodium metal batteries (SMBs) is hampered due to the inferior interfacial stability between Na metal and conventional electrolytes. Therefore, a high-concentration electrolyte is proposed to solve this issue. However, high viscosity, low ionic conductivity, and unsatisfactory wettability toward the separator need to be overcome. In this study, a localized high-concentration electrolyte (LHCE) is formulated with 1 wt% SbF₃ as an interface-stabilized additive to protect the Na metal anode. This reformulated LHCE retains the special coordination structure in HCE with improved wettability and high ionic conductivity. Moreover, the introduction of the SbF₃ additive into the LHCE resulted in a bilayer-structured solid electrolyte interface (SEI) including a Na–Sb alloy inner layer and a NaF-rich outer layer on the Na metal. As expected, the Na‖Na cells using LHCE + 1 wt% SbF₃ show a long cycle lifespan of over 1200 h at 0.5 mA·cm⁻² with negligible polarization, and Na‖Na₃V₂(PO₄)₃ cells exhibit a high capacity exceeding 97 mAh·g⁻¹ at 40C.

Keywords Sodium metal battery; Localized high-concentration electrolyte; SbF₃ additive; Wettability; Conductivity

W. Fang, R. Jiang, H. Zheng, Y. Zheng, Y. Sun, X. Liang, H.-F. Xiang*
School of Materials Science and Engineering, Engineering Research Center of High Performance Copper Alloy Materials and Processing, Ministry of Education, Hefei University of Technology, Hefei 230009, China
e-mail: hfxiang@hfut.edu.cn

Y.-Z. Feng
Key Laboratory of Materials Processing and Mold, Ministry of Education, Zhengzhou University, Zhengzhou 450002, China

Y. Yu*
Hefei National Laboratory for Physical Sciences at the Microscale, Department of Materials Science and Engineering, Key Laboratory of Materials for Energy Conversion, Chinese Academy of Sciences (CAS), University of Science and Technology of China, Hefei 230026, China
e-mail: yanyumse@ustc.edu.cn

Y. Yu
Dalian National Laboratory for Clean Energy (DNL), Chinese Academy of Sciences (CAS), Dalian 116023, China

1 Introduction

Owing to the high natural abundance of Na [1–3] and its similar chemistry to lithium [4–7], rechargeable sodium (Na) batteries have become one of the most promising energy storage technologies used to meet the increasing demands for large-scale grids. Compared with carbon-based anodes with relatively low capacity and high cost, Na metal anode is competitive due to its high specific capacity (1165 mAh·g⁻¹) and the low redox potential (− 2.714 V vs. a standard hydrogen electrode) [8–12]. Nevertheless, the application of Na metal still faces some challenges due to its high reactivity with conventional liquid electrolytes and the instability of the solid electrolyte interface (SEI) [13], along with Na dendrite growth [14, 15], resulting in inferior cell performance and safety concerns [16–22].

To solve the problems caused by the intensive reactivity of Na metal, various strategies have been proposed, among which electrolyte modification is one of the most effective and convenient approaches [23, 24]. Recently, high-concentration electrolytes (HCEs) have gained much attention

due to their impressive ability to the improvements in interfacial stability [25]. Contact ion pairs and aggregate solvates are the main solvation forms in HCE so that reactivity of solvents and anion in the electrolyte can be effectively reduced. In addition, the increased concentration of Na^+ promotes the uniform plating/stripping of Na. Zhang et al. reported that the 4 $mol \cdot L^{-1}$ Na bis(fluorosulfonyl) imide (NaFSI) in 1,2-dimethoxyethane (DME) enabled stable cycling with superior average coulombic efficiency (CE) (> 99%) in Na‖$Na_3V_2(PO_4)_3$ cells [25]. In our recent research, the HCE electrolyte with SbF_3 additive contributed to a bilayer-structured SEI with a Na–Sb alloy inner layer and a NaF-rich outer layer on the Na metal surface. The Na‖Na cells delivered steady cycling for nearly 1000 h with negligible voltage polarization at 0.5 $mA \cdot cm^{-2}$ [26]. Nevertheless, the large-scale application of HCE is still restricted due to its high viscosity and poor wettability which result in its low ionic conductivity. Most recently, 'inert' diluents, which were different from conventional co-solvents, were added into the HCE to overcome these problems and form a localized high-concentration electrolyte (LHCE) [27]. The diluents have little influence on the solvation structure in localized regions; thus, the LHCE has comparable interfacial stability with the corresponding HCE [28]. Furthermore, lower Na salt concentration in LHCE enables reduced bulk viscosity, enhanced wettability, and increased ionic conductivity of LHCE [29].

In this work, we reformulate an LHCE composed of 2 $mol \cdot L^{-1}$ NaFSI/DME + 1,1,2,2-tetrafluoroethyl 2,2,3,3-tetrafluoropropyl ether (FEPE) with 1 wt% SbF_3 additive, where FEPE is a diluent due to its low dielectric constant and low donor number [30]. SbF_3 acts as an interface-stabilized additive, which helps to fabricate an alloy-phase inner interfacial layer to suppress the Na dendrite growth, and LHCE leads to a smooth NaF-rich outer layer. The combination of SbF_3 additive and LHCE contributes to the formation of a bilayer-structured SEI on the surface of the Na metal, which effectively inhibits the continuous interfacial side reactions and enhances the electrochemical performance of sodium metal battery (SMBs) (Fig. 1).

## 2 Experimental

2.1 Electrolyte preparation

The HCE with 4 $mol \cdot L^{-1}$ NaFSI/DME was obtained from Anhui Sage Energy Technology Co., Ltd. The FEPE was obtained from Tokyo Chemical Industry (TCL). The LHCE composed of 2 $mol \cdot L^{-1}$ NaFSI/DME + FEPE (1:1, molar ratio) and LHCE + 1 wt% SbF_3 was prepared in an MBraun glove box with the oxygen and moisture less than 0.1×10^{-6}.

2.2 Characterization

The ionic conductivity of the electrolytes was measured using a DDS-307A conductivity meter (Leici Co., Ltd.) at 25 °C. To evaluate the wettability of each electrolyte, the electrolytes were dropped on a glass fiber separator (GF/D, Whatman). Scanning electron microscope (SEM, JEOL JSM-6390LA) was used to observe the surface morphology of the cycled Na metal after 100 h, and energy dispersive X-ray spectroscopy (EDS) mappings were used to analyze the existence and location of elements of the Na metal surface.

2.3 Electrochemical measurements

For the purpose of assessing the electrochemical stability of each electrolyte, the Na‖Na and Na‖$Na_3V_2(PO_4)_3$ (denoted as NVP) cells were assembled using the glass fiber separator, and 80 µl electrolyte was added into each cell. The NVP cathode was manufactured by mingling NVP, super-P and polyvinylidene fluoride (PVDF) with the mass ratio of 8:1:1 in N-methyl-2-pyrrolidone (NMP), and the slurry was applied to aluminum foil. The NVP cathode was
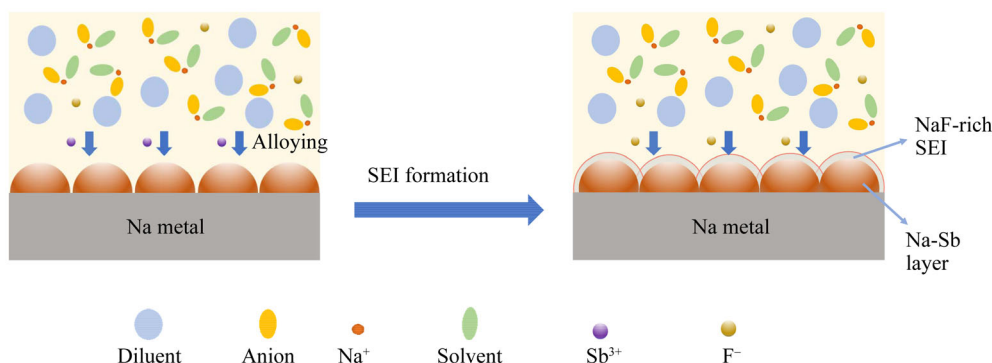
Fig. 1 Schematic diagram of SEI formation mechanism by using LHCE + 1 wt% SbF_3

made into a disk with a diameter of 14 mm (mass loading of 9.6 mg) after drying for 6 h at 60 °C. For the Na metal anode, the passivation layer on the sodium surface was removed by a knife and also made into disks (Φ14 mm).

For Na||NVP full cells, all the cells were cycled under a current of 2C (0.31 mA·cm^{-2}) after initial cycles at 0.1C between 2 and 4 V. The rate performance of the Na||NVP cells was assessed with a fixed charge current of 1C and discharged at various rates of 1C, 10C, 20C, 30C and 40C for five cycles (25 °C). To examine the interfacial stability, alternative current (AC) impedance measurements were carried out using a CHI660e electrochemical workstation in the frequency range from 1×10^{-2} to 1×10^{5} Hz.

3 Results and discussion

To evaluate the wettability of each electrolyte, the electrolytes were dropped on the glass fiber separator. As shown in Fig. 2a, c, the HCE shows poor wettability toward the separator due to its high viscosity, while the LHCE exhibits superior wettability (Fig. 2b, d), indicating that FEPE dilution could significantly improve the wettability toward the separator [30]. In addition, the ionic conductivity of LHCE is obviously increased compared to that of the HCE electrolyte (Fig. 2e). Thus, the presence of FEPE enables the electrolytes to have better separator wettability and higher ionic conductivity, which ensures the superior electrochemical performance of SMBs.

The plating/stripping behavior of Na in each electrolyte was examined using symmetric cells at a current density of 0.5 mA·cm^{-2}. As shown in Fig. 3a, the cell with HCE has a short lifespan of 400 h with polarization voltage increasing, and this kind of voltage spike is a sign of uneven Na deposition. In comparison, the cell using LHCE delivers a lower overpotential and remains stable over 1000 h. Generally, the enhanced cycling performance of Na||Na symmetric cells corresponds to the smoother Na plating/stripping. According to previous studies [28, 30], the improved cycling stability in LHCE compared to that of HCE is attributed to improved wettability, lower viscosity, and higher conductivity caused by FEPE diluent. After the addition of SbF$_3$, the cell using LHCE + 1 wt% SbF$_3$ shows superior cycling stability (over 1200 h) with lower polarization. Figure 3b, c shows zoomed graphics in view of Fig. 3a, in which the lower overpotential of the cell using LHCE + 1 wt% SbF$_3$ can be significantly observed. Similar to our previous work on HCE [26], the introduction of SbF$_3$ into LHCE results in a bilayer-structured solid electrolyte interface including a Na–Sb alloy inner layer and a NaF-rich outer layer on the Na metal. Herein, the excellent electrochemical stability is mainly attributed to the following reasons: (1) the tough alloy layer can inhibit the growth of dendrites on the surface of Na metal; (2) the hard alloy layer provides a stable base for the formation of the outer NaF-rich SEI; (3) this Na–Sb alloy layer can reduce the Na$^+$ diffusion barrier and allow uniform ion transmission [31, 32]. In addition, the NaF-rich layer also enhances the interfacial stability. Thus, the NaF/Na–Sb bilayer structure ensures fast ion transfer and negligible polarization.

The influence of each electrolyte on the surface morphologies of Na metal was characterized by SEM. The top view of the Na metal was acquired from Na||Na symmetric cells after cycling. As shown in Fig. 4a, the morphologies of Na metal cycled in HCE show a relatively irregular growth of some protrusions. Such an uneven surface is not conducive to the uniform deposition of Na$^+$ and finally leads to the dendrites growth. In contrast, the cell with the LHCE electrolyte exhibits a flat surface, indicating that a more robust SEI is formed. However, there are still some cracks with particles of impurities (Fig. 4b). As shown in
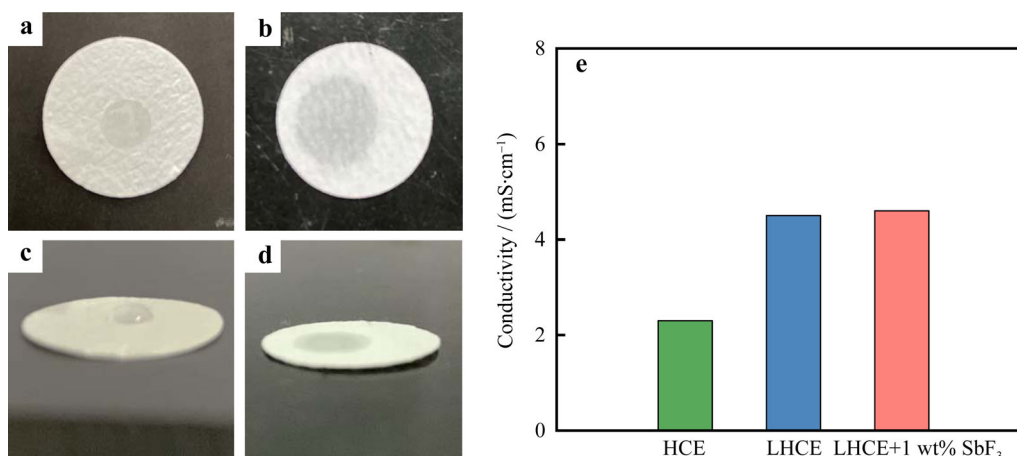
Fig. 2 Wettability of **a**, **c** HCE and **b**, **d** LHCE toward separator; **e** ionic conductivity of different electrolytes at 25 °C
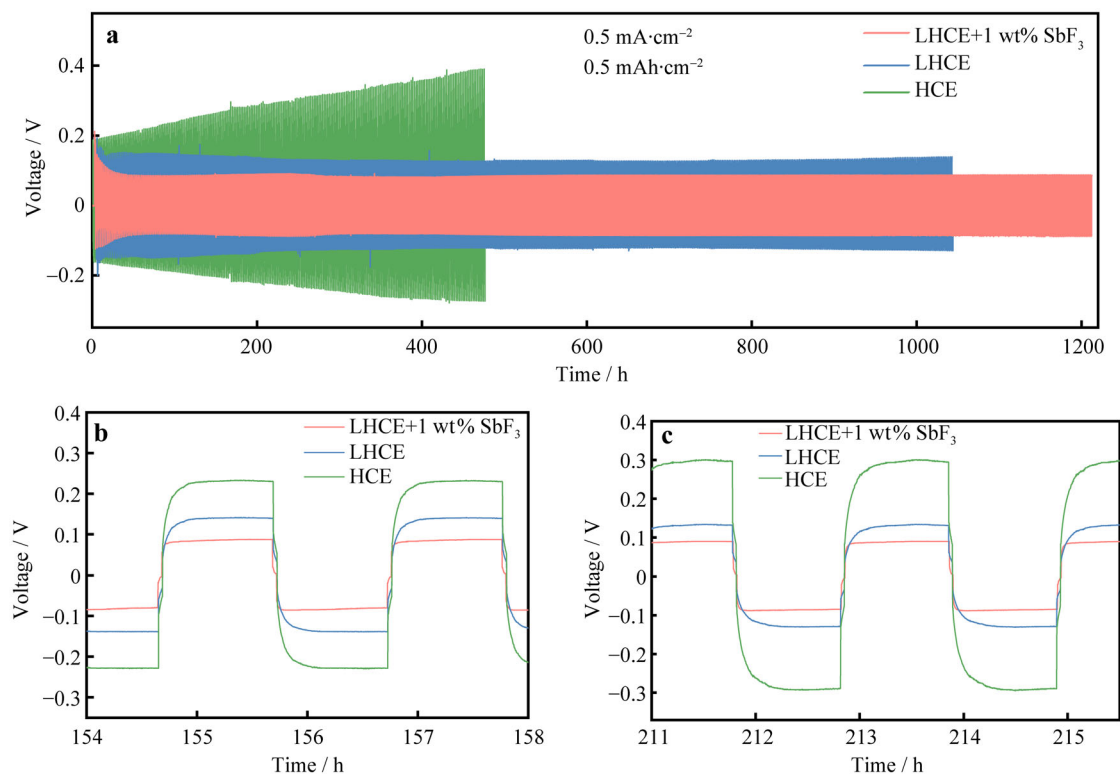
Fig. 3 **a** Cycling capacity of Na‖Na symmetric cells using various electrolytes at 0.5 mA·cm^{-2}; **b**, **c** partially enlarged voltage profiles of **a**
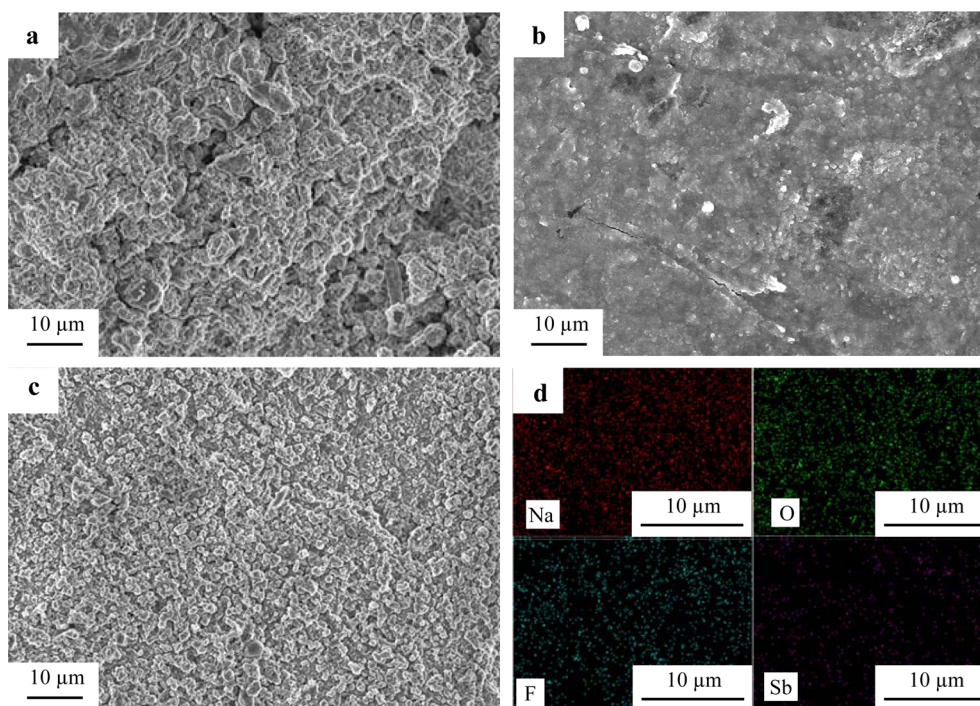
Fig. 4 SEM images of cycled Na metal with **a** HCE, **b** LHCE and **c** LHCE + 1 wt% SbF$_3$ after 100 h; **d** EDS spectra of Na metal cycled in LHCE + 1 wt% SbF$_3$ electrolyte with Na, O, F and Sb signals

Fig. 4c, the surface is covered with a layer of dense alloy particles after introducing SbF$_3$ into LHCE. EDS elemental mappings further confirm the existence of Sb and F, which indicate the formation of Na–Sb alloy and NaF-rich layers.

This morphology formed in LHCE + 1 wt% SbF_3 exhibits a smoother surface, resulting in the more facile interfacial ion transport and dendrite-free Na deposition. These results are also consistent with the electrochemical performance of the symmetric cells.

The cycling stability of Na‖NVP cells using various electrolytes was tested at 2C in the voltage range of 2-4 V. As shown in Fig. 5a, after the initial formation cycles at 0.1C, the Na‖NVP cells containing different electrolytes exhibit similar specific capacities of 112 mAh·g^{-1}. The capacity of the cell containing HCE electrolyte decreases to 89 mAh·g^{-1} during 1000 cycles, leaving only 79% of its initial discharge capacity. The capacity of the cell using the LHCE electrolyte deteriorates tardily, and the capacity retention is 87% (98 mAh·g^{-1}) after 1000 cycles. In contrast, due to the formation of a robust SEI and uniform ion transmission, the cell with LHCE + 1 wt% SbF_3 demonstrates the best capacity retention of 95% after 1000 cycles. Figure 5b shows the coulombic efficiency (CE) of various electrolytes during the first 20 cycles. The CE of the cells
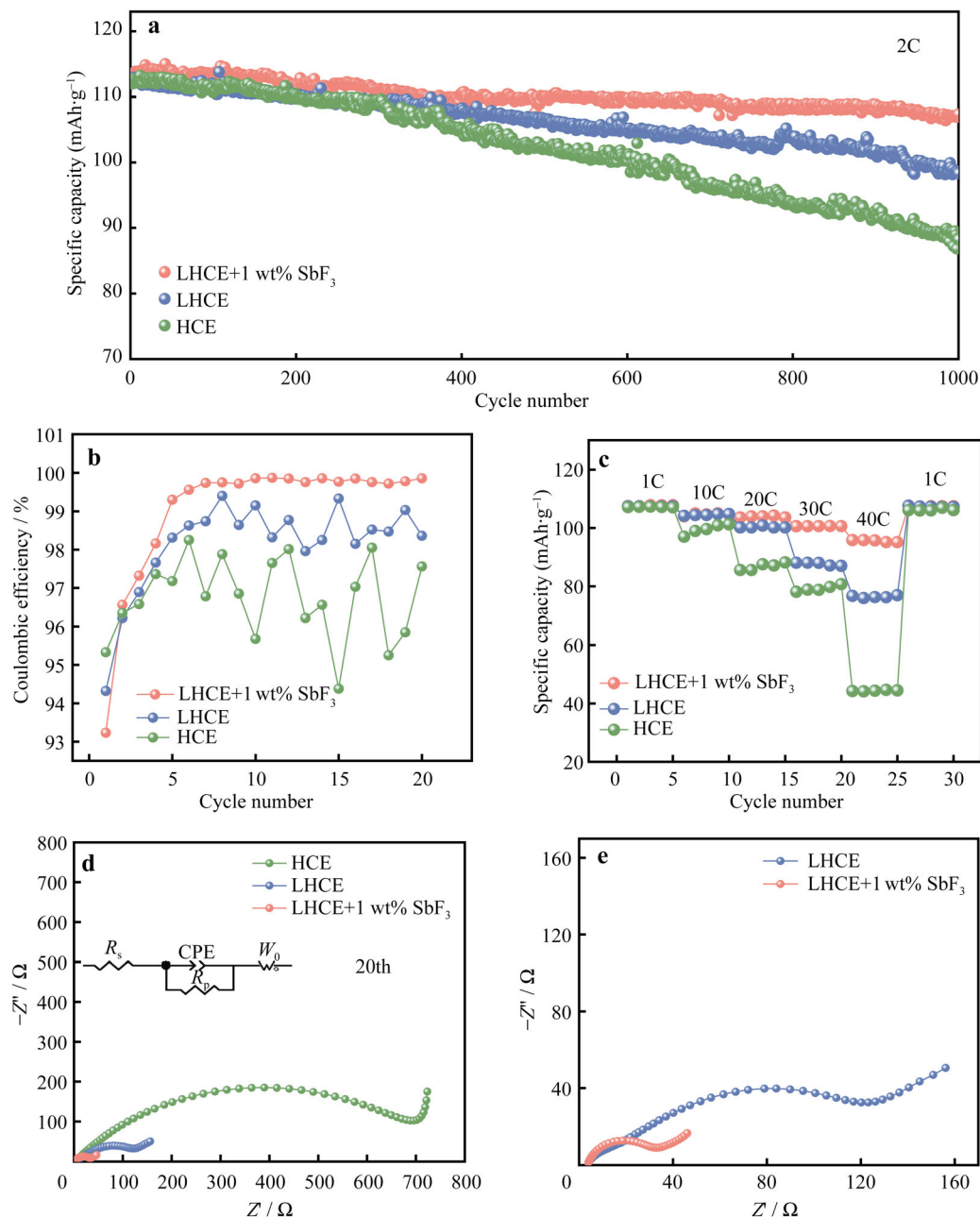
Fig. 5 a Cycling performance and b Coulombic efficiency of HCE, LHCE and LHCE + 1 wt% SbF_3 electrolytes; c rate performance of Na‖NVP cells using various electrolytes; d Nyquist plots of Na‖NVP battery with each electrolyte after 20 cycles; e zoomed Nyquist plots of LHCE and LHCE + 1 wt% SbF_3

containing LHCE + 1 wt% SbF$_3$ reaches 99% rapidly after the formation cycles, indicating the superior electrode reaction kinetics [30]. In addition, its lowest initial CE represents the irreversible consumption of Na for the formation of the SEI [29]. Figure 5c shows the rate ability of Na||NVP cells with different electrolytes. The cell using LHCE + 1 wt% SbF$_3$ delivers capacities of 107, 105, 103, 100, and 97 mAh·g^{-1} at current rates of 1C, 10C, 20C, 30C, and 40C, respectively. As for the cell using LHCE, the capacity decreases to 107, 104, 100, 86, and 76 mAh·g^{-1} at the same current density. The cell with HCE electrolyte performs even worse with discharge capacities of 107, 99, 85, 78, and 44 mAh·g^{-1}. The impedance was investigated by electrochemical impedance spectroscopy (EIS). The abscissa and ordinate in the EIS spectrum represent the impedance of real and imaginary part. R_s, R_p, CPE, and W_0 represent the ohmic impedance of the electrolyte, the charge transfer, the adsorption of the surface, and the diffusion resistance of sodium ions inside the electrode, respectively [33]. The cell with HCE shows the highest R_p (688 Ω) due to the poor interfacial reaction kinetics of HCE [30]. In contrast, the cell using LHCE drops to 125 Ω because of its higher ionic conductivity. In comparison, the impedance drops significantly (29 Ω) after the addition of 1 wt% SbF$_3$, which is attributed to a bilayer-structured SEI and facile ion surface diffusion [26, 34].

4 Conclusion

To summarize, the FEPE diluent not only enables LHCE to preserve the original solvent structure of HCE, but also helps to improve the interfacial reaction kinetics of the Na metal anode. Moreover, introduction of the SbF$_3$ additive into the LHCE results in a bilayer-structured SEI, including a Na–Sb alloy inner layer and a NaF-rich outer layer on the Na metal, which insures the dendrite-free Na plating and fast interfacial ion transport. As a result, the Na||NVP cells exhibit stable cycling over 1000 cycles with a capacity retention of 95% and deliver a discharge capacity of 97 mAh·g^{-1} even at the high rate of 40C due to the synergy of LHCE and SbF$_3$. This formula of electrolyte holds great potential for the next-generation SMBs with high energy densities and promotes the practical application of SMBs.

References

[1] Yang J, Wan HL, Zhang ZH, Liu GZ, Xu XX, Hu YS, Yao XY. NASICON-structured Na$_{3.1}$Zr$_{1.95}$Mg$_{0.05}$Si$_2$PO$_{12}$ solid electrolyte for solid-state sodium batteries. Rare Met. 2018;37(6):480.

[2] Xu K. Nonaqueous liquid electrolytes for lithium-based rechargeable batteries. Chem Rev. 2004;104(10):4303.

[3] Li F, Wei ZX, Manthiram A, Feng YZ, Ma JM, Mai LQ. Sodium-based batteries: from critical materials to battery systems. J Mater Chem A. 2019;7(16):9406.

[4] Peng Z, Song JH, Huai LY, Jia HP, Xiao BW, Zou LF, Zhu GM, Martinez A, Roy S, Murugesan V, Lee H, Ren XD, Li QY, Liu B, Li XL, Wang DY, Xu W, Zhang JG. Enhanced stability of Li metal anodes by synergetic control of nucleation and the solid electrolyte interphase. Adv Energy Mater. 2019;9(42):1901764.

[5] Yun FL, Tang L, Li WC, Jin WR, Pang J, Lu SG. Thermal behavior analysis of a pouch type Li[Ni$_{0.7}$Co$_{0.15}$Mn$_{0.15}$]O$_2$-based lithium-ion battery. Rare Met. 2015;35(4):309.

[6] Li KK, Zhang J, Lin DM, Wang DW, Li BH, Lv W, Sun S, He Y-B, Kang FY, Yang QH, Zhou LM, Zhang TY. Evolution of the electrochemical interface in sodium ion batteries with ether electrolytes. Nat Commun. 2019;10(1):725.

[7] Chen D, Tan HT, Rui XH, Zhang Q, Feng YZ, Geng HB, Li CC, Huang SM, Yu Y. Oxyvanite V$_3$O$_5$: a new intercalation-type anode for lithium-ion battery. InfoMat. 2019;1(2):251.

[8] Kim H, Park I, Lee S, Kim H, Park KY, Park YU, Kim H, Kim J, Lim HD, Yoon WS, Kang K. Understanding the electrochemical mechanism of the new iron-based mixed-phosphate Na$_4$Fe$_3$(PO$_4$)$_2$(P$_2$O$_7$) in a Na rechargeable battery. Chem Mater. 2013;25(18):3614.

[9] Ponrouch A, Monti D, Boschin A, Steen B, Johansson P, Palacín MR. Non-aqueous electrolytes for sodium-ion batteries. J Mater Chem A. 2015;3(1):22.

[10] Lee J, Lee Y, Lee J, Lee SM, Choi JH, Kim H, Kwon MS, Kang K, Lee KT, Choi N-S. Ultraconcentrated sodium bis(fluorosulfonyl)imide-based electrolytes for high-performance sodium metal batteries. ACS Appl Mater Int. 2017;9(4):3723.

[11] Wang JL, Yang J, Nuli YN, Holze R. Room temperature Na/S batteries with sulfur composite cathode materials. Electrochem Commun. 2007;9(1):31.

[12] Mao ML, Luo C, Pollard TP, Hou S, Gao T, Fan XL, Cui CY, Yue JM, Tong YX, Yang GJ, Deng T, Zhang M, Ma JM, Suo LM, Borodin O, Wang CS. A pyrazine-based polymer for fast-charge batteries. Angew Chem. 2019;58(49):17820.

[13] Rui XH, Sun WP, Wu C, Yu Y, Yan QY. An advanced sodium-ion battery composed of carbon coated Na$_3$V$_2$(PO$_4$)$_3$ in a porous graphene network. Adv Mater. 2015;27(42):6670.

[14] Zhu MQ, Li SM, Li B, Gong YJ, Du ZG, Yang SB. Homogeneous guiding deposition of sodium through main group II metals toward dendrite-free sodium anodes. Sci Adv. 2019;5(4):6264.

[15] Zhang D, Wang S, Li B, Gong YJ, Yang SB. Horizontal growth of lithium on parallelly aligned Mxene layers towards dendrite-free metallic lithium anodes. Adv Mater. 2019;31(33):1901820.

[16] He Y, Ren XD, Xu YB, Engelhard MH, Li XL, Xiao J, Liu J, Zhang J-G, Xu W, Wang CM. Origin of lithium whisker formation and growth under stress. Nat Nanotechnol. 2019;14(11):1042.

[17] Kim H, Jeong G, Kim YU, Kim JH, Park CM, Sohn HJ. Metallic anodes for next generation secondary batteries. Chem Soc Rev. 2013;42(23):9011.

[18] Zhao CL, Lu YX, Yue JM, Pan D, Qi YR, Hu YS, Chen LQ. Advanced Na metal anodes. J Energy Chem. 2018;27(6):1584.

[19] Cao X, Xu YB, Zhang LC, Engelhard MH, Zhong LR, Ren XD, Jia HP, Liu B, Niu CJ, Matthews BE, Wu HP, Arey BW, Wang CM, Zhang JG, Xu W. Nonflammable electrolytes for lithium ion batteries enabled by ultraconformal passivation interphases. ACS Energy Lett. 2019;4(10):2529.

[20] Zhao CL, Liu LL, Qi XG, Lu YX, Wu FX, Zhao JM, Yu Y, Hu YS, Chen LQ. Solid-state sodium batteries. Adv Energy Mater. 2018;8(17):1703012.

[21] Jiang ZY, Wang SQ, Chen XZ, Yang WL, Yao X, Hu XC, Han QY, Wang HH. Tape-casting $Li_{0.34}La_{0.56}TiO_3$ ceramic electrolyte films permit high energy density of lithium–metal batteries. Adv Mater. 2019;32(6):1906221.

[22] Wei ZH, Ren YQ, Sokolowski J, Zhu XD, Wu G. Mechanistic understanding of the role separators playing in advanced lithium-sulfur batteries. InfoMat. 2020;2(3):483.

[23] Eshetu GG, Martinez-Ibanez M, Sanchez-Diez E, Gracia I, Li CM, Lide M, Rodriguez-Martinez Rojo T, Zhang H, Armand M. Electrolyte additives for room-temperature, Sodium-based, rechargeable batteries. Chem Asian J. 2018;13(19):2770.

[24] Zeng ZQ, Liu XW, Jiang XY, Liu ZJ, Peng ZQ, Feng XM, Chen WH, Xia DG, Ai XP, Yang HX, Cao YL. Enabling an intrinsically safe and high-energy-density 4.5 V-class Li-ion battery with nonflammable electrolyte. InfoMat. 2020;2(5):1.

[25] Cao RG, Mishra K, Li XL, Qian JF, Engelhard MH, Bowden ME, Han KS, Mueller KT, Henderson AW, Zhang J-G. Enabling room temperature sodium metal batteries. Nano Energy. 2016; 30:825.

[26] Fang W, Jiang H, Zheng Y, Zheng H, Liang X, Sun Y, Chen CH, Xiang HF. A bilayer interface formed in high concentration electrolyte with SbF_3 additive for long-cycle and high-rate sodium metal battery. J Power Sources. 2020;455:227956.

[27] Ren XD, Chen SR, Lee H, Mei DH, Engelhard MH, Burton SD, Zhao WG, Zheng JM, Li QY, Ding MS, Schroeder M, Alvarado J, Xu K, Meng S, Liu J, Zhang JG, Xu W. Localized high-concentration sulfone electrolytes for high-efficiency lithium-metal batteries. Chem. 2018;4(8):1877.

[28] Yu L, Chen SR, Lee H, Zhang LC, Engelhard MH, Li QY, Jiao SH, Liu J, Xu W, Zhang JG. A localized high-concentration electrolyte with optimized solvents and lithium difluoro(oxalate)borate additive for stable lithium metal batteries. ACS Energy Lett. 2018;3(9):2059.

[29] Doi T, Shimizu Y, Hashinokuchi M, Inaba M. Dilution of highly concentrated $LiBF_4$/propylene carbonate electrolyte solution with fluoroalkyl ethers for 5-V $LiNi_{0.5}Mn_{1.5}O_4$ positive electrodes. J. Electrochem. Soc. 2017;164(1):6412.

[30] Zheng JM, Chen SR, Zhao WG, Song JH, Engelhard MH, Zhang JG. Extremely stable sodium metal batteries enabled by localized high-concentration electrolytes. ACS Energy Lett. 2018; 3(2):315.

[31] Tu ZY, Choudhury S, Zachman MJ, Wei SY, Zhang KH, Kourkoutis LF, Archer LA. Fast ion transport at solid–solid interfaces in hybrid battery anodes. Nat Energy. 2018;3(4):310.

[32] Liang X, Pang Q, Kochetkov IR, Sempere MS, Huang H, Sun XQ, Nazar LF. A facile surface chemistry route to a stabilized lithium metal anode. Nat Energy. 2017;2(9):17119.

[33] Zheng XY, Fu HY, Hu CC, Xu H, Huang Y, Wen JY, Sun HB, Luo W, Huang YH. Toward a stable sodium metal anode in carbonate electrolyte: a compact, inorganic alloy interface. J Phys Chem Lett. 2019;10(4):707.

[34] Xu ZX, Yang J, Zhang T, Sun LM, Nuli YN, Wang JL, Hirano S. Stable Na metal anode enabled by a reinforced multistructural SEI layer. Adv Funct Mater. 2019;29(27):190.